Estimation of Time–Temperature-Transformation Diagrams of Mold Powder Slags from Thermo-analysis of Non-isothermal Crystallization

YADIRA G. MALDONADO, CLAUDIA BARRAZA DE LA P., SERGIO RODRÍGUEZ A., A. HUMBERTO CASTILLEJOS E., and BRIAN G. THOMAS

The temperature range across the mold powder slag in the interfacial gap between the continuous casting mold and strand leads through different transformation behavior into crystalline phases. The transformation rates play a key role in determining the proportion of glassy and crystalline phases present, and thus greatly influence mold heat transfer and lubrication. Although thermal analysis has held great promise to quantify the crystallization of mold slags, so far the information it has provided is scarce. This work shows how differential scanning calorimetry, DSC, data allow evaluation of Time–Temperature-Transformation, TTT, diagrams of mold powder slags, when analyzed with the induction period and the Kissinger methods. The data required for estimating this important tool for the analysis and design of mold powders are onset temperature, T_i, peak maximum temperature, T_m, shape index, S, and conversion at peak maximum, x_m, of the crystallization peaks appearing on thermograms obtained at various heating and cooling rates, ϕ or $-\phi$, respectively. Industrial mold powders for casting low- and medium-carbon steels were analyzed to obtain TTT diagrams which correctly portray their different crystallization behavior. The diagrams reveal the start and end curves of the crystalline phases forming at each DSC crystallization peak. The estimated TTT curves present a correct picture of the degree of transformation observed in glass disks (~3 mm thick) treated isothermally for specified time intervals, quenched and examined with a scanning electron microscope. Additionally, the procedure developed for DSC-based TTT diagram calculation is supported by the good agreement between expected transformations and qualitative or quantitative X-ray diffraction results obtained from mold glass-powdered samples treated isothermally in a muffle furnace.

DOI: 10.1007/s11663-014-0185-x

I. INTRODUCTION

THE mold is the most crucial component of the steel continuous casting machine. The rate and uniformity of heat removal from the strand, especially near the meniscus, controls the surface quality of the product and the stability of the process. An excessive and/or uneven rate of heat extraction from the newly solidified shell may induce thermal stresses that ultimately cause longitudinal cracks.[1] On the other hand, insufficient heat removal may lead to relatively weak spots in the shell, possibly leading to breakouts.[2] Rejection or reconditioning of cracked slabs causes considerable yield losses,[3] and a slab breakout is a major process upset with grave safety hazards, machine damage, and line stoppage.[4] Thus, interfacial heat transfer must harmonize with the operation conditions, *e.g.*, steel composition, casting speed and mold design. This must be achieved by controlling the characteristics—conductivity and thickness—of the layers in the mold-strand gap.

These layers are a slag film in contact with the strand and an air gap or contact resistance between it and the mold. The slag film is made of a liquid and a solid layer, and the latter may have both glassy and crystalline phases accommodated in different and complex fashions or can be fully glassy or crystalline.[5–13] Heat is transferred through the mold strand gap by conduction and radiation through the liquid and solid slag layers and air gap which act as a series of thermal resistances. Heat transfer is dominated by radiation and conduction in parallel through the liquid slag layer and by conduction through the glassy-and-crystalline solid layers.[9,14–19] The interfacial air-gap resistance amounts to ~50 pct

YADIRA G. MALDONADO, Formerly Ph.D. Graduate with the Laboratory of Process Metallurgy, Department of Metallurgical Engineering, Centro de Investigación y de Estudios Avanzados, CINVESTAV – Unidad Saltillo, Av. Industria Metalúrgica 1062, Parque Industrial Saltillo-Ramos Arizpe, 25900 Ramos Arizpe, Coahuila, Mexico, is now Surface Analysis and Nanometrology Specialist with the Centro Nacional de Metrología, Querétaro, Mexico. CLAUDIA BARRAZA DE LA P., M.Sc. Graduate, SERGIO RODRÍGUEZ A., Research Assistant, and A. HUMBERTO CASTILLEJOS E., Professor, are with the Laboratory of Process Metallurgy, Department of Metallurgical Engineering, Centro de Investigación y de Estudios Avanzados, CINVESTAV – Unidad Saltillo. Contact e-mail: humberto.castillejos@cinvestav.edu.mx BRIAN G. THOMAS, C.J. Gauthier Professor, is with the Department of Mechanical Science and Engineering, University of Illinois at Urbana-Champaign, 1206 West Green Street, Urbana, IL 61801.

Manuscript submitted June 16, 2014.
Article published online September 25, 2014.

for powders used to cast low-carbon steels, LC, and to ~60 pct for powders employed for casting medium-carbon steels, MC.[15] The radiative conduction resistance is sensitive to the amount of crystallization[15] and is larger for MC than LC slags due to the higher tendency of MC powders to crystallize.[16] Radiative heat transfer is smaller for MC powders because more crystals are present to enhance scattering and refraction.[17–19] In addition, greater crystallization causes a larger contraction of the solid flux layer which leads the solid surface facing the mold to become rougher and hence a larger contact resistance[8,9,16,18]; the transformation of glass to slightly denser crystalline phases causes pores to form inside the solid layer, which lower heat transfer.[8,20]

Thus, the crystallization of the slag film in the mold-strand gap deserves a great deal of attention. The formation of crystals during cooling of liquid slag or during heating of glass (formed from liquid slag quenching) may be classified, respectively, as crystallization and devitrification. In the commercial continuous casting process, the average cooling rates of the mold slag have been claimed to be approximately −20 to −25 K/s (−1200 to −1500 °C/min) with local cooling rates as high as around −50 to −100 K/s (−3000 to −6000 °C/min).[21] Cooling rates near the mold wall may be far higher than the critical cooling rates of liquid slags,[5–8] *i.e.*, higher than the slowest rate at which a melt can be cooled from its liquidus temperature (T_L) to below the glass transition temperature, T_g, without detectable crystallization. Consequently, the formation of a solid glass phase is favored initially.[5–8] However, the temperature of the slag film on the mold side could range between 573 K and 773 K (300 °C and 500 °C),[9] so devitrification would occur if the glass layer stays long enough in the mold.[5–8] On the hot face of the slag film, in contact with the steel shell, temperatures decrease from the steel liquidus temperature at the meniscus to ~1273 K or ~1423 K (1000 °C or 1150 °C) for thin[22] and conventional molds,[2] respectively, which often enables crystals to form in the liquid phase (crystallization).

To learn about the distribution of glassy and crystalline phases, the degree of crystallization and the film thickness under actual casting conditions, slag film samples have been gathered from the mold wall[6–8,10] or from a collecting device placed at the mold exit.[11,12] These samples vary from highly crystalline to fully glassy and usually exhibit a crystalline layer on the mold wall side.[6] However, the opposite was found in slag for peritectic grade steels.[11] Complex bands of crystallized/glassy phases are often present in different combinations due to both the slag properties and locally varying in-mold conditions, such as powder melting rate, molten slag infiltration and element pick-up.[8,10,11] The slag film is rather thin, with thicknesses between 0.25 and 4 mm,[11] or even finer (0.05 and 0.5 mm).[12]

Although the teachings of the industrial trials are of great relevance, the intense pressure on productivity makes highly desirable the availability of laboratory methods that can provide a good measure of in-mold powder behavior.[25] The glass and crystalline fractions of in-mold samples are often characterized by differential thermal analysis, DTA, comparing the areas under the exothermic peaks for these samples against those of pure glass samples of the same slag.[23] DTA of fresh glass samples and of samples taken from the top of the mold at different times from the start-up of the casting sequence revealed that the thermograms change with time, displaying one peak for unused and two peaks for used powders, but both samples presented the same two crystalline phases.[24] It has been claimed that DTA methods offer the best approach to determine the crystallization temperature of mold powders[25] and to define the extent of crystallization.[26] However, the thermoanalytical methods still do not meet the expectations and several others have arisen.[13,20,27–42]

With the lack of standardized tests, different techniques often lead to disagreeing results on crystallization behavior,[25,26] hindering design, selection, use, and quality control of mold powders. Thus, a negative event arising after opening a new batch of the same powder is commonly attributed to a change in powder properties, such as a change in its mineralogical constitution.[11] However, unless the powder did not fully melt, it is difficult to understand how changing only the powder minerals could change the slag behavior. Situations like this clearly highlight the importance of having laboratory tests that can accurately evaluate crystallization characteristics, including comparison of batches of the 'same' powder, and thereby isolate endogenous from exogenous causes of suspected crystallization problems.

A simple test consists in pouring molten slag into a mold for visual or microscopic examination of the solidified sample. Test conditions such as mold temperature greatly affect the behavior. A mold temperature of 883 K (610 °C) with a holding time of 1200 seconds (20 minutes) produced crystallization percentages similar to samples from an actual process; while mold temperatures of ~288 K (~15 °C) led to much less crystallization.[27] This finding is consistent with model calculations that contact resistance at the mold wall of the real process can keep the slag temperature above 900 K (627 °C) at 0.1 mm from the hot face.[9] The test based on dipping a water cooled plate into molten slags generated crystals near the plate after just 10 seconds in some slags, while others stayed glassy after 30 seconds.[28]

Another test is to continuously record the temperature during cooling of a molten sample.[20] A change in slope of the cooling curve indicates the release of the exothermic heat of crystallization and corresponds to a crystallization temperature. This temperature was found to increase with basicity (*i.e.*, pct CaO/pct SiO_2) of the slag, and the increase was also associated with a higher area percentage of pores in the solid slag.[20]

A more fundamental understanding of transformation during cooling of liquid slags is obtained from TTT curves. These curves can be obtained by isothermally holding a molten slag sample long enough to homogenize its composition and temperature before quenching to the test temperature, maintaining for a specified time and rapidly quenching to ambient. Crystallization can be observed after the treatment[29] or in real-time during

the test.[13,30–42] Measuring after quenching to ambient over-estimates transformation, because the interrupted quench can take 5 to 10 seconds.[29] Real-time methods, such as single-hot thermocouple technique, SHTT,[30–34] double-hot thermocouple technique, DHTT,[13,34–38] and confocal laser scanning microscope, CLSM,[39–42] allow cooling rates as high as −150 K/s (−9000 °C/min), so there is less transformation during cooling to the isothermal test temperature. DHTT additionally allows imposing temperature gradients across the slag film as occurs in the real process. Care must be taken to prevent or account for unintended gradients.[38] In addition to the cooling rate, humidity is another important exogenous variable that can greatly affect crystallization kinetics. DHTT tests in dry and humid atmospheres showed that water vapor caused the nucleation and growth rates of crystals to increase significantly.[35,36] Other DHTT tests revealed that crystallization is strongly dependent on the specific details of the cooling path. These findings could explain why two casters operating under similar conditions with the same powder can experience considerably different heat transfer and lubrication behavior.[35]

In thermo-analysis tests [*e.g.*, DTA and differential scanning calorimetry (DSC)], typical heating and cooling rates range between 0.017 and 1 K/s (1 and 60 °C/min) which are much smaller than those achieved in SHTT, DHTT, CLSM or a muffle furnace. Hence, these methods should not use simple isothermal analysis methodologies owing to the transformations occurring prior to the isothermal treatment. Thus, several researchers have processed non-isothermal DTA results that offer useful insights into the crystallization behavior of mold slags.[23,24,43–47] Using the maximum peak temperature of the dominant exotherm from DTA curves obtained with different heating rates, the activation energy, E, for devitrification has been evaluated as 100 to 450 kJ/mol and it has been claimed that increases with increasing viscosity and decreasing basicity.[43] Comparative DTA measurements during cooling at −0.25 K/s (−15 °C/min) showed that increased addition of MnO to a slag caused a considerable decrease in crystallization temperature, and also the authors reported a decrease in viscosity.[44] Devitrification must play a major role in the plant environment, because more crystals were found in plant samples than in DTA samples cooled slowly at −0.5 to −0.83 K/s (−30 to −50 °C/min) from the molten state.[45]

DSC has also been used to analyze the thermal behavior of mold slags during crystallization and devitrification.[48–50] In studies involving different batches of the same powder, the tests showed similar peak temperatures along the devitrification path but along the crystallization path the peak temperatures were different for different batches and some batches did not show a peak.[11,49] These differences in crystallization were attributed to variations in the mineralogical make-up of the powder[11] and to small differences in composition that changed the phases precipitating from the slag[49] However, cooling molten oxides often exhibit a small heat of crystallization or a slow crystallization rate that hampers the detection of crystallization peaks in DTA and DSC, while the peaks during non-isothermal devitrification on a solid glass of the same material are detectable.[51] Thus, it is critical to determine the actual cause of the differences in DTA or DCS crystallization curves, because the sensitivity and resolution of these instruments is affected by several factors, *e.g.*, scan rate, sample size, purge gas, pan material, and sample-pan contact.[52]

Although thermo-analysis by DSC or DTA is the most widely used method to characterize the crystallization behavior of mold powders, the information it has provided is limited compared with other techniques. Thus, the current work was undertaken to extend the use of DSC to evaluate TTT diagrams of mold powder slags, by further analysis of the DSC traces with the induction period and the Kissinger methods. The data required for this new tool are onset temperature, T_i, peak maximum temperature, T_m, shape index, S, and conversion at peak maximum, x_m, of the crystallization peaks appearing on thermograms obtained at various heating and cooling rates, ϕ or $-\phi$, respectively. The new DSC-estimated TTT diagrams are then validated by comparison with results of isothermal tests evaluated with X-ray diffraction measurements and with micrographs of samples at different stages during crystallization, to demonstrate the great potential value of the new method.

II. THEORETICAL FRAMEWORK

Many different thermo-analysis methods [*e.g.*, DSC, DTA, and thermogravimetry (TG)] have been use to study the kinetics of reactions in different materials, *e.g.*, glass–ceramics, metallic-glasses, metallic alloys, glasses, oils, polymers, carbonates and silicates, among others.[53–71] Most studies involve non-isothermal conditions because many reactions occur before a prescribed isothermal condition could be reached. In these non-isothermal methods, the instrument measures a response variable, *e.g.*, temperature, heat flux or weight, during the temperature history and interprets its changes as proportional to the changes in the fraction reacted as a function of temperature, T, or time, t. The data is analyzed to extract reaction kinetic parameters such as activation energy, E, pre-exponential or frequency factor, A, and order of reaction exponent, n. Among several methods, the Kissinger method,[53,54,65] is the most popular.[58,60] This method estimates the activation energy from plots of logarithms of the ratio of heating rate over the squared absolute temperature at the maximum reaction rate *vs* the inverse of these temperatures, obtained from thermograms generated under linear heating rate conditions. This method was initially derived to study the thermal decomposition of a solid into another solid and a gas where the steps of nucleation and growth were not considered.[66] However, many works have validated its adequacy for analyzing the crystallization process of glass and other solid-state transformations.[55,56,58–60,64]

The reaction/transformation rate is expressed as the product of two independent functions denoted as $k(T)$

and $f(x)$, the first depending only on absolute temperature, $T(K)$, and the second on the fraction reacted or transformed, x, as follows,

$$\frac{dx}{dt} = k(T)f(x). \quad [1]$$

This mathematical expression is not connected easily to the fundamental reaction mechanisms but can be fit to reproduce observed behavior by extracting kinetic parameters from the thermo-analysis traces. The Arrhenius expression ($= A\ e^{(-E/RT)}$) is commonly used as $k(T)$, thus giving,

$$\frac{dx}{dt} = Ae^{(-E/RT)}f(x) \quad [2]$$

while several algebraic expression have been used to specify the kinetic model $f(x)$,[60,63] including the following expression of Kissinger,[54]

$$f(x) = (1-x)^n, \quad [3]$$

where $n = 1$ for a first-order reaction. Assuming that the non-isothermal process involves heating or cooling with a linear temperature variation, $|\phi|$ ($= dT/dt$), Eq. [2] gives,

$$\frac{dx}{dt} = \frac{A}{|\phi|}e^{-E/RT}f(x), \quad [4]$$

where dx/dT represents the variation of the fraction reacted with temperature, as given by a non-isothermal thermo-analysis technique.

A. *Induction Period Method*

Before transformation begins, many processes exhibit an induction period, IP, which is not detected by the experimental measurements, but occurs to form nuclei of critical size. Šimon *et al.*[67–71] have presented models to describe isothermal and non-isothermal IP.

The induction period method of Šimon[67–71] is an isoconversional method to perform kinetic analysis from fixed value conversions obtained from a set of thermo-analysis runs. The first detectable manifestation of the IP occurs at its end or equivalently the start of the main transformation process, given by an initial conversion fraction x_i, which is assumed to be the same for any temperature. This fraction is reached at time, t_i, at which the onset temperature, T_i, of the exothermic crystallization peak first starts in the thermo-analysis trace, *i.e.*, at the begging of the steep temperature rise. Separating variables and rearranging terms in Eq. [2] to integrate within the limits of the IP leads to the following expression,

$$\int_0^{x_i} \frac{dx}{f(x)} = \int_0^{t_i} \frac{dt}{\frac{e^{(E_i/RT)}}{A_i}}, \quad [5]$$

where E_i and A_i are, respectively, the activation energy and frequency factor of the process taking place during the IP. Further, integrating the l.h.s. term of the equation and introducing the variables,

$$A_i' = \frac{F(x_i) - F(0)}{A_i}\ ;\ B_i = E_i/R. \quad [6]$$

Equation [5] can be written as,

$$1 = \int_0^{t_i} \frac{dt}{A_i' e^{(B_i/T)}}. \quad [7]$$

Under isothermal conditions the integrand in Eq. [7] is constant and therefore the induction time t_i is given as,

$$t_i = A_i' e^{(B_i/T)}. \quad [8]$$

Assuming that the process taking place during the induction period is the same at any temperature, then the constants A_1' and B_i can be obtained from non-isothermal thermal-analysis tests carried out at constant heating rate, ϕ ($= dT/dt$), by rearranging and integrating Eq. [7], to give

$$\phi = \int_0^{T_i} \frac{dT}{A_i' e^{(B_i/T)}}. \quad [9]$$

When heating (devitrification), the lower limit in the integral of Eq. [9] is 0 K (−273 °C), as no transformation would take place at this temperature. When cooling from a melt ϕ is negative, so in this work Eq. [9] was written as,

$$\phi = \int_{T_L}^{T_i} \frac{dT}{A_i' e^{(B_i/T)}} \quad [10]$$

for crystallization processes, where T_L is the liquidus temperature at which no crystallization would occur.

The parameters A_1' and B_i are computed by minimizing the sum of the squares of the differences between experimental and computed values of the onset temperature T_i for various ϕ. For this, a program was adapted to accomplish this function minimization using the Simplex method of Nelder and Mead[72] written by Shaw[73] and amended by Miller.[73] The computed A_1' and B_i parameters are substituted in Eq. [8] to estimate t_i as function of T.

B. *Kissinger Method*

The Kissinger method[53,54,64,65] is based on recognizing that the maximum of the peaks in a thermogram experiences a time displacement with increasing heating rate and hence is classified as a peak maximum evolution method. Additionally, it assumes that at the peak maximum the reaction rate is maximum and therefore $(d^2x/dt^2)_m = 0$. Hence, differentiating Eq. [2] with respect to t, the following expression is obtained after evaluating the function at the peak maximum,

$$\frac{E_k}{RT_m^2}\phi = -A_k\left(\frac{df(x)}{dx}\right)_m e^{(-E_k/RT_m)} \quad [11]$$

Taking natural logarithms of both sides of this equation and substituting the first derivative of Eq. [3] give,

$$\ln\frac{\phi}{T_m^2} = \ln\left(\frac{A_K R}{E_K} n(1-x)_m^{n-1}\right) - \frac{E_K}{R}\frac{1}{T_m} \quad [12]$$

For a process showing a constant conversion fraction at the maximum of a DSC peak—peak maximum for short—obtained at different heating rates, the first term on the r.h.s. of Eq. [12] is constant. The volume fraction of crystals at the peak maximum, x_m, can be obtained from DSC curves through the following expression,

$$x_m = \frac{S_m}{S_T} \quad [13]$$

where S_T is the area between the DSC peak trace and the baseline, during the entire crystallization process and S_m is the area between those two curves, from the start of crystallization at T_i to the peak maximum at T_m. When x_m is constant, Eq. [12] represents a linear relationship between $\ln(\phi/T_m^2)$ and $1/T_m$. Thus, the activation energy E_K can be calculated from the slope of Eq. [12] and the frequency factor A_K from the abscissa and the order of reaction n. In this work the following expression of Kissinger[54] was used to evaluate n,

$$n = 1.26\left|\frac{\left(\frac{d^2x}{dt^2}\right)_1}{\left(\frac{d^2x}{dt^2}\right)_2}\right|^{1/2} = 1.26S^{1/2} \quad [14]$$

where the second derivatives correspond to the slopes of the tangents at the inflection points of the thermoanalysis peak and S is called the peak shape index.

During cooling transformations (crystallization), the Kissinger equation can be rewritten as follows to avoid numerical problems,

$$\ln\frac{|\phi|}{T_m^2} = \ln\left(\frac{A_K R}{|E_K|} n(1-x)_m^{n-1}\right) - \frac{E_K}{R}\frac{1}{T_m} \quad [15]$$

Of course, this form is valid also during heating.

C. *Evolution of the Degree of Conversion Under Isothermal Conditions*

Substituting in Eq. [2] the n-order kinetic model proposed by Kissinger[54] gives the following expression for the variation of the fraction transformed with time,

$$\frac{dx}{dt} = [A_K e^{-B_K/T}](1-x)^n \quad [16]$$

For an isothermal process the term in brackets is constant, so Eq. [16] can be rewritten in integral form as,

$$\int_{x_i}^{x}\frac{dx}{(1-x)^n} = [A_K e^{-B_K/T}]\int_{t_i}^{t} dt \quad [17]$$

Considering that $x_i \approx 0$, the time, t, required to obtain a certain degree of transformation, x, at a given temperature, T, is given as

$$t = t_i + \left(\frac{1-(1-x)^{1-n}}{[A_K e^{-B_K/T}]}\right)\left(\frac{1}{1-n}\right) \quad [18]$$

In this work, DSC thermograms obtained at various constant heating and cooling rates are used to extract values of T_i, T_m, S, and x_m to calculate the kinetic parameters for: (a) the induction period, *i.e.*, A_1' and B_i (required for the evaluation of t_i), and (b) the crystal growth period, *i.e.*, A_K, E_K, and n, which are required for the calculation of TTT diagrams according to Eq. [18].

III. EXPERIMENTAL

A. *Materials and Glass Sample Preparation*

Commercial mold powders used for casting CSP thin steel slabs were selected for the study. The powder denoted as A is used for casting low-carbon steels and powder B for casting medium-carbon steels. A bag of 25 kg of each powder was decarburized in porcelain lab dishes with a capacity of 0.10 kg. Several dishes at a time were heated in a resistance muffle furnace at 873 K (600 °C) for 16 hours, with interruptions after 5 and 10 hours to mix the powder, in order to insure complete C removal. Afterwards the decarburized powder was ground in an Al_2O_3 ball mill to a mesh size of −100 (≤149 μm). The total amount of the ground powder obtained for each mold flux was put in a sealed bucket where it was homogenized using a drum rolling mixer. During storing of the powder desiccant material was placed inside the bucket to minimize exposure to humidity.

Samples of ~19 g of ground decarburized powder were melted and held for 300 seconds (5 minutes) at 1573 K (1300 °C) in a graphite crucible heated by induction. This time and temperature were selected short and low to minimize weight losses by evaporation of volatile species, but at the same time the slag was sufficiently fluid for easy homogenization and pouring into a mold. Brass molds (~0.014 m dia. × 0.06 m hgt.) heated with an electric resistance to a temperature of around ~373 K (~100 °C) were used to solidify fully glassy rods without experiencing thermal shock.[74] Using a zero background holder for placing ground rod material X-ray diffraction showed that the starting samples used in all the tests (*i.e.*, DSC tests, isothermal annealing tests in muffle furnace and quasi-isothermal annealing tests in XRD heating chamber) were amorphous. This can be appreciated by the diffraction

pattern presented in Figure 1 for glass A, which shows no specific peak and exhibits the characteristic hump of a glassy material, which appeared between 27 and 37 deg 2θ; glass B exhibited a similar pattern. The average chemical compositions of the glass samples prepared from powder A and B are reported in Table I.

B. *Differential Scanning Calorimetry Tests*

Non-isothermal simultaneous DSC/TGA tests were conducted using an SDT-Q600 apparatus (TA Instruments, New Castle, DE). The instrument is a heat flux type DSC that is regularly calibrated. Heat flow, temperature difference, and weight variations associated with the transformations taking place in initially glassy slag samples, in powder form, were recorded as a function of temperature and time. The thermal cycles consisted of imposing different linear heating rates from 673 K to 1473 K (400 °C to 1200 °C), followed by holding for 600 seconds (10 minutes) and then cooling to 673 K (400 °C) at the same absolute rate, and finally freely cooling to ambient. However, it should be mentioned that due to the formation of volatile species, weight losses between ~1 and ~8 pct were measured at the fastest and slowest heating rates, respectively; during the cooling path weight losses were much smaller. However, it must be noticed that the holding temperature selected was just above the liquidus temperature of the mold powder slags and the holding time was relatively short, but long enough to destroy all traces of previous crystalline order. Smaller times resulted in weaker crystallization peaks during cooling,[75] perhaps because the crystalline order of the phases formed during heating had not disappeared.

The samples for the DSC tests were prepared by grinding parts of the glass rods, described in Section III–A, to sizes between −230 and +270 mesh (*i.e.*, ≤63 to ≥53 μm). For glass A, the heating, holding and cooling paths, *i.e.*, the paths for devitrification, melt stabilization and crystallization, were consecutive and the samples weighted ~65 mg in all the tests. For glass B the devitrification and crystallization tests were run on separate samples, using weights of ~15 mg for heating paths and ~65 mg for cooling paths. The reason for using a smaller weight during devitrification of glass B, which has a large tendency to crystallize, is that its transformation is so energetic that the rate of heating of the sample exceeded the programmed rate, causing a loss of control in the temperature program which led to a very irregular peak shape[75]; the possible reason is given in Section IV–A. In all the tests powdered Al_2O_3 was used as the reference material and the purging gas was dry nitrogen at a flow rate of 1.67 mL/s (100 mL/min). Pt crucibles, 0.006 m dia. × 0.004 m hgt., were used and the heating and cooling rates employed ranged from 0.083 to 0.83 K/s (5 to 50 °C/min), the specific values are given in Section IV–A together with the thermograms obtained in each of the tests. Data from the thermograms were analyzed according to the procedures described in Section II to extract the parameters to estimate TTT diagrams.

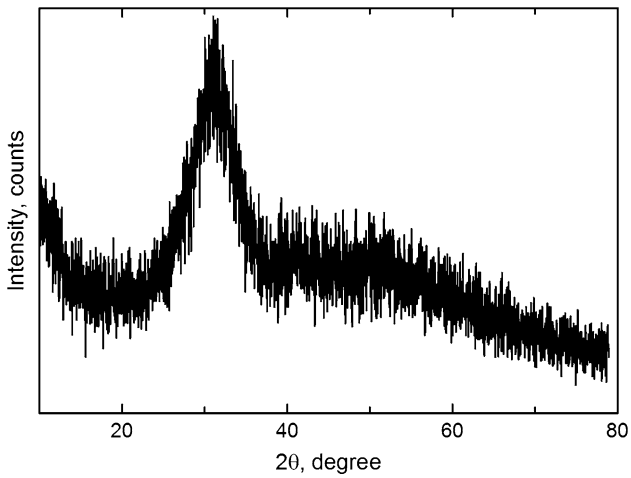

Fig. 1—XRD pattern of a typical A glassy slag sample.

C. *Isothermal Treatment Tests*

To validate the new DSC-based TTT diagrams, independent tests were conducted to approximate isothermal transformation conditions by rapid heating of each sample to a desired temperature, where it was held for predetermined times, and quenched to ambient. Two different kinds of samples were used: (a) glass disks ~3.1 mm thick, cut from the rods manufactured as described in Section III–A, and (b) glass powdered samples like those used in the DSC tests but weighting 1 g.

The glass disk is placed on an Inconel 601 holder that is inductively heated as shown in Figure 2. The heater used a three-turns flat induction coil energized by a high frequency, HF, generator (Luzarz URF-5, ASEPSA S.A. de C.V. QRO., Mexico) with a capacity of 5 kW. As seen in Figure 2 the heating pan was instrumented with a K-type thermocouple connected to a controller interfaced to the HF generator. The controller is programed to follow devitrification treatments such as the one shown in Figure 3(a). In each test, the Inconel plate, with the glass disk on top, was heated from room temperature to 573 K (300 °C) in 30 seconds and held for 60 seconds. This temperature plateau avoided thermal shock of the sample and was too low and short to cause crystallization or even nucleation, because this was below the glass transition temperature. Then, the plate was heated to the chosen isothermal test temperature in 13 seconds (independently of the temperature chosen) for the desired time, after which the disk was cooled rapidly. The temperatures and times of each isothermal treatment are given in Section IV–C together with the photomicrographs obtained from scanning electron microscope, SEM, analysis of the test samples.

Before each devitrification test, the Inconel plate was polished with 800 and 1200 emery papers and the transverse surfaces of the glass disk were polished up to colloidal silica suspension of 0.05 μm. The glass disk encased in a thermally insulating ceramic ring was placed on the pan, and a contact thermocouple was seated on its exposed top surface, as sketched in Figure 2. Measurement of this surface temperature

Table I. Basicity and Composition of Glass Samples Prepared from Mold Powders A and B

Powder	pctCaO/pctSiO_2	pctSiO_2	pctCaO	pctMgO	pctAl_2O_3	pct(Na_2O + K_2O)	pctMnO	pctF
*A	0.94	37.0	34.8	3.8	3.3	13.6	—	7.6
**B	1.08	31.6	34.2	3.7	6.8	10.5	3.7	9.0

The *F* was analyzed by the Seel method and the other elements by XRF. Viscosity at 1573 K (1300 °C): *0.9 dPa s; **0.7 dPa s.

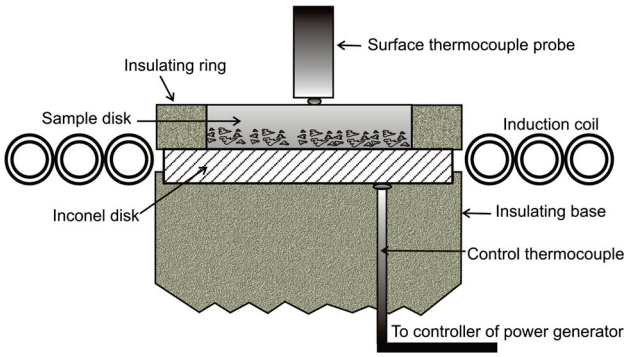

Fig. 2—Experimental arrangement for isothermal testing of glass disks.

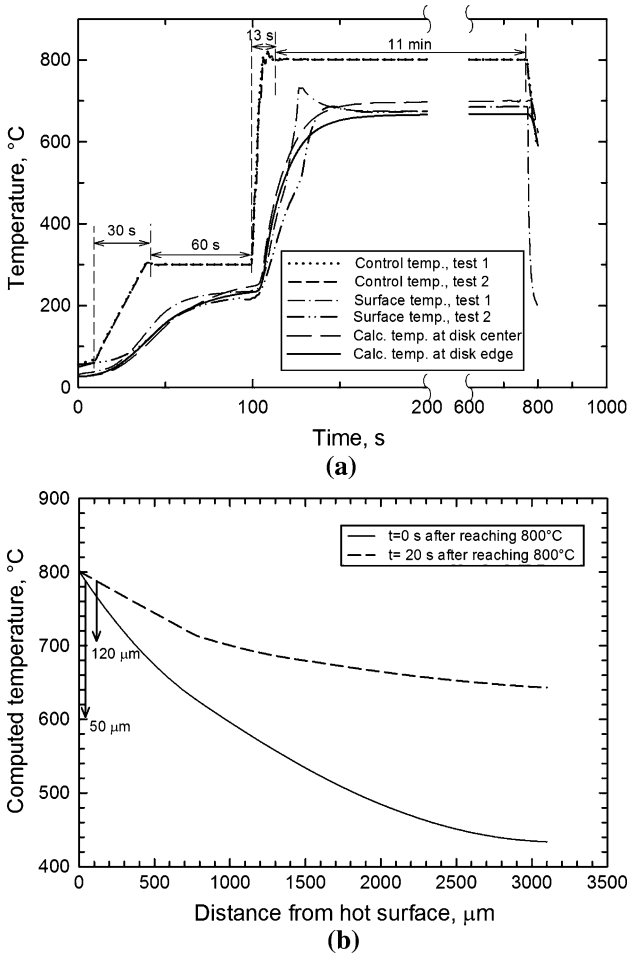

Fig. 3—(*a*) Measured and computed temperature histories for: Inconel plate (control temperature) and at top surface of glass disk (surface temperature) and (*b*) axial temperature profiles predicted at the start of the isothermal plateau and 20 s (0.33 min) later. Both isothermal treatments were at 1073 K (800 °C) lasting 660 s (11 min).

allowed calibration of a 2D axisymmetric computational finite-element model of transient heat-conduction in the disk, which was used to calculate temperature histories at different disk locations and the axial thermal profiles at different times. Details of the model built in Comsol are given elsewhere.[75]

Figure 3(a) shows, for a particular experiment, the temperature measured by the control thermocouple as a function of time, together with measured and computed temperature evolution curves of the center and edge of the top surface of the glass disk. The calculated temperature curves lie very close to the measured ones, and this was the case in all the experiments. Figure 3(b) shows axial temperature profiles for the moment when the control thermocouple reached 1073 K (800 °C) and 20 seconds later. The model predicts that after a very short time, a 50 μm thick region at the hot disk surface is very close to the desired temperature. Based on these calculations, to follow the progress of devitrification, metallographic observations were carried out only in the 50 μm region where isothermal conditions were closely approximated. After the isothermal treatment time elapsed, the sample was removed rapidly from the Inconel plate and was left to cool down without the insulating ring under a gentle air stream. The disks were mounted on epoxy resin to study the longitudinal cross section near the hot surface. That section surface was polished up to colloidal silica suspension of 0.05 μm, etched with a Nital 2 pct solution for 3 seconds, and examined in the SEM.

The isothermal tests with powdered glass were done by introducing 1-g samples in a Pt pan into a muffle furnace that was preheated to the desired temperature. After the sample was introduced, time was given for the furnace to recover to the test temperature before starting to count the desired isothermal holding time. Then, the sample was rapidly removed, and left to cool down in air. The samples were analyzed by X-ray diffraction using a Philips X'Pert diffractometer, with a θ to 2θ Bragg–Bretano geometry. In order to determine the precipitated crystalline phases and their proportion in the mixtures obtained after the thermal treatments, diffraction data collection was carried by Cu radiation in the angular range of 7 to 100 deg 2θ with steps of 0.025 deg 2θ and a counting time of 16.5 s/step. The relative weight percentages of the crystalline phases present were determined through a Rietveld refinement procedure of the pattern.

D. *Quasi-isothermal Treatment Tests*

The diffractometer is equipped with a heating chamber (HTK 16, Anton Paar), that can reach a maximum temperature of 1773 K (1500 °C), and can replicate the

heating and cooling rates used in the DSC tests. Thus, to determine the crystalline phases associated with the peaks appearing in the non-isothermal DSC devitrification traces, samples of ~1 g of the powdered A and B glasses were heated to selected temperatures within the range of those peaks. The heating rate was 0.33 K/s (20 K/min), which is intermediate among those used in the DSC tests. Each sample was then held for a short time before cooling rapidly [at around −8.33 K/s (−500 °C/min)] to room temperature. The crystalline phases found in the quenched samples were identified and quantified using the XRD conditions described in Section III–C. The holding temperatures and times used in the treatments are given in Section IV–A.

IV. RESULTS AND DISCUSSION

A. *DSC Thermograms*

The formation of a crystalline phase is an exothermic process that generates a peak in a DSC trace obtained during the thermal treatment of a glass sample. The DSC traces showing the peaks associated with the crystalline transformations experienced with different heating and cooling rates are shown in Figures 4(a) and (b) for glass A and in Figures 4(c) and (d), for glass B. During heating, all of the traces exhibit, before the crystallization peaks, a slope change that corresponds to glass transition, *i.e.*, to the region where the rigid glass network acquires mobility and becomes plastic. The change in slope appears as a peak on the curve of the first derivative of the DSC trace,[76] and the peak temperature on this curve was taken as the glass transition temperature, T_g. The glass transition temperatures increase with increasing ϕ as indicated by the line drawn in Figures 4(a) and (c). Note that T_g is smaller for glass B which has a higher basicity and a smaller viscosity than glass A, as seen in Table I, and thus becomes plastic more easily. The T_g depends on the glass composition, and decreases in the presence of silicate network breaking cations, such as Ca^{2+}.[18] During heating, these cations lead to shorter networks, facilitating the transition of a brittle glass to a relatively fluid supercooled liquid. As seen in Table I, in addition to the larger CaO/SiO_2 ratio, glass B has higher contents of fluorine and manganese that might have lowered the viscosity,[42,44,45,78] which led to the smaller T_g.

Figure 4 shows that the onset and maximum of the crystallization peaks shift to higher temperatures as the heating rate increases and to lower temperatures as the cooling rates increase, complying with a requirement of the methods described in Section II. The increase of the peak maximum with heating rate is due to the time needed for the kinetically controlled reaction to proceed. As the heating or cooling rate increases, the material spends less time at a given temperature, so the reaction is delayed. The delay time varies greatly according to the temperature-dependent rates of induction and growth of the crystalline phases. In each case, however, the onset and maximum of the crystallization peaks are delayed toward higher or lower temperatures depending on the trajectory and the peak height increases as needed to achieve the same degree of conversion at peak maximum, according to the Kissinger method.[53,54]

During devitrification tests, exothermic peaks were detected for all the heating rates tested, as seen in Figures 4(a) and (c). However, this regularity in the curves was not observed during crystallization, when cooling from the molten state, as Figures 4(b) and (d) have some curves with no peaks; even though visual observation suggested that crystallization took place, as confirmed in some cases by XRD. This behavior has been observed in cooling melts that have a small heat of crystallization or a very slow crystallization rate, such as would be expected at cooling rates approaching the critical value.[51] However, the cooling rates achieved in DSC are much smaller than the critical rates for the mold slags under study, and peaks were sometimes absent at intermediate rates, in addition to the highest rates. This suggests that the cause was a poor thermal contact of the sample with the pan during cooling from the molten state. In fact, several samples showed a fluffy appearance, hinting at poor contact with the pan base. Most likely, this also caused the absence of crystallization peaks that were attributed to changes in the powder mineralogy.[11,49] Perhaps this problem could be remedied by encapsulation of the sample to ensure better thermal contact with the pan and pan holder; this kind of tests and others are underway in the laboratory of the authors. Nonetheless a sufficient number of DSC curves were obtained during cooling for calculating the kinetic parameters needed to estimate TTT diagrams according to the procedures described in Section II, as will be presented in Sections IV–B and IV–C.

Figures 4(a) and (c), respectively, show that during devitrification of the LC-steel glass A two peaks appeared while the MC-steel glass B presented just one. On the other hand, during crystallization, when cooling from the molten state, slag A showed just one peak and slag B exhibited four as seen in Figures 4(b) and (d), respectively. The number of peaks in a thermogram does not always reveal the number of crystalline phases or compounds that precipitated, because the number of peaks and the way they evolve are very sensitive to: chemical composition, kinetics of crystals evolution, thermal conditions and environmental conditions affecting nucleation.

The quasi-isothermal tests described in Section III–D were designed to determine the crystalline phase or phases associated to the devitrification peaks of both glasses. Figure 5(a) shows the DSC devitrification curve obtained with glass A when using a heating rate of 0.33 K/s (20 K/min), together with dotted lines indicating the end temperatures used in the quasi-isothermal tests. As seen in figure, two temperatures fell within the temperature range of $P_{h,1}$ [898 K and 923 K (625 °C, 650 °C)] and one [948 K (675 °C)] within the range of $P_{h,2}$. At these test temperatures the samples were held for 60 seconds (1 minute), except for the highest temperature which was also held for 300 seconds (5 minutes). The as-quenched samples were analyzed by XRD and the patterns obtained are shown in Figure 5(b), from the patterns is seen that $P_{h,1}$ was the result of the

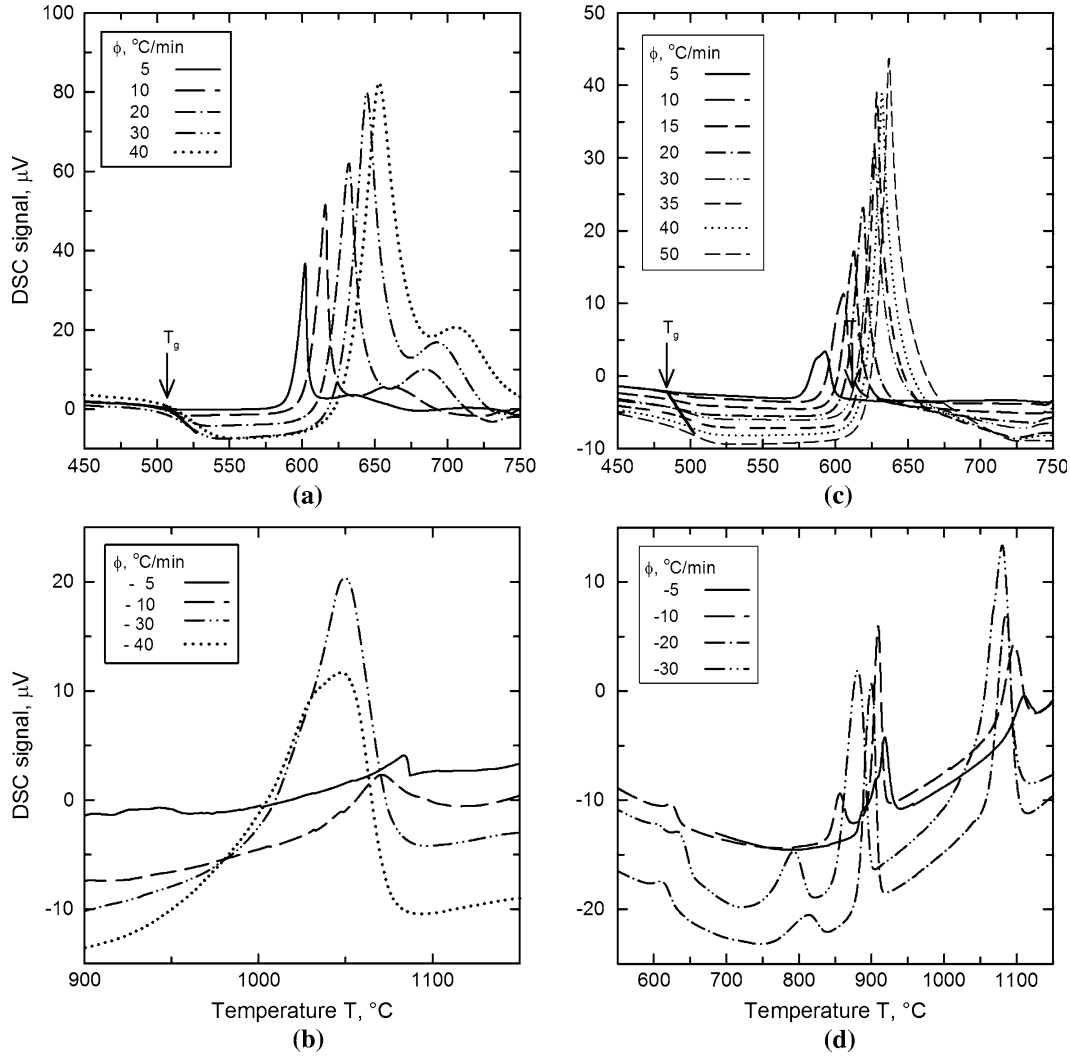

Fig. 4—DSC traces for heating and cooling at constant rates indicated: (*a*) devitrification (heating) and (*b*) crystallization (cooling) of slag A; and (*c*) devitrification and (*d*) crystallization of slag B.

formation of cuspidine, and $P_{h,2}$ originated from the formation of combeite. In the case of the samples held 1 minute at the indicated temperatures the XRD patterns present remains of the characteristic hump of the amorphous glassy flux that was shown in Figure 1, but for 300 seconds (5 minutes) of holding at 948 K (675 °C) the hump disappeared. The XRD results and the relative proportions of the crystalline phases found at the different test conditions are reported in Table II.

For glass B the holding temperatures selected for the quasi-isothermal tests were 883 K, 893 K and 903 K (610 °C, 620 °C, 630 °C), all of which are within the temperature range of the only one peak that appeared during the devitrification of this glass. The as-quenched samples from these tests were studied by XRD, and the results are reported in Table III. From table is seen that the only one peak appearing during devitrification was associated to the formation of four crystalline phases: cuspidine, quartz, sodium aluminosilicate, and mullite; also is seen that the proportions of these crystalline phases evolved during heating; two phases increased and two decreased. With so many phases forming simultaneously, it is conjectured that the energetic heat release was responsible for the irregular DSC signal that appeared when using samples of 65 mg of glass B, as was mentioned in Section III–B. The large heat release increased the rate of heating of the sample above the programed rate. This was the reason for using small samples of just 15 mg for studying the devitrification of this glass.

Figures 4(a) and (c) also show that the onset and peak maximum temperatures of the devitrification peak of slag B are slightly smaller than those for peak 1 of slag A, hinting its larger tendency to devitrify. On the other hand, the onset and peak maximum temperatures of peak 1 for the crystallization of slag B during cooling tests were considerably higher than those of slag A at all cooling rates, which reveals a larger tendency to crystallize when starting from the liquid state. Additionally, three other crystallization peaks appeared at relatively low temperatures.

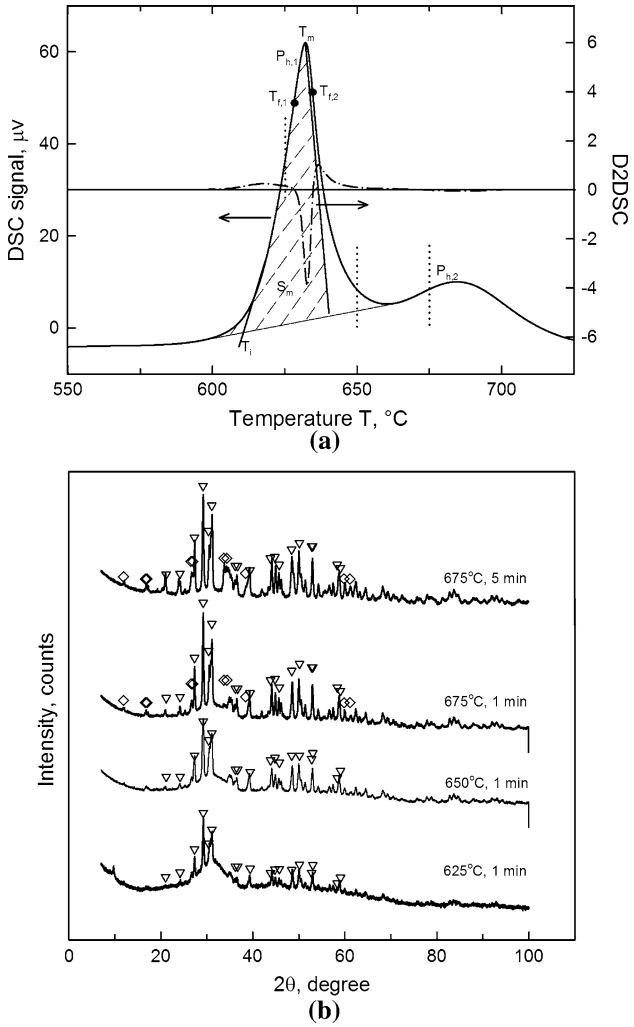

Fig. 5—(*a*) DSC trace for glass A for a heating rate of 0.33 K/s (20 °C/min), showing: second derivative of the signal, onset temperature, T_i, peak maximum temperature, T_m, temperatures at inflection points, $T_{f,1}$, $T_{f,2}$ and area at peak maximum, S_m; (*b*) XRD patterns of specimens quenched after staying at given temperatures for specified times, the heating rate to the indicated temperatures was 0.33 K/s (20 °C/min); triangles indicate peaks of cuspidine and diamonds of combeite.

B. *Kinetic Parameters*

1. *Induction period*

To characterize the start of crystallization it is necessary to evaluate the kinetic parameters that define the duration t_i of the induction period that precedes it and where little transformation takes place, such that $x_i \approx 0$. As described in Section II–A, the method presented by Šimon and Kolman[67] was applied to evaluate the modified activation energy B_i and the modified frequency factor A_i' needed to define the duration of the induction period of the transformations associated with all of the peaks appearing in the non-isothermal DSC tests carried out at constant heating rate and at constant cooling rate, using the onset temperatures of all these peaks.

Specifically, a Simplex method program[73] was adapted to find the parameters A_i' and B_i that minimized the sum of the squares of the differences between the experimentally measured T_i and the T_i values computed with either Eq. [9] (for devitrification heating tests) or Eq. [10] (for crystallization cooling tests) at the various ϕ used in the DSC tests. This fitting procedure was done for the inductions periods preceding each of the peaks in the heating and cooling DSC traces of slags A and B.

The agreement between experimental and computed T_i *vs* ϕ points for slag A are displayed in Figures 6(a) and (b) for the two peaks that appeared during heating and in Figure 6(c) for the peak developed during cooling. From figures, is seen that the fitting is very good for the induction periods preceding the devitrification processes and reasonable for those of the crystallization treatments. Similar agreement was obtained for glass B.[75] The values of A_i' and B_i that satisfied the fitting procedure are listed in Table IV for each of the peaks, and were used in Eq. [8] to estimate the length of the induction period, t_i.

2. *Crystallization period*

Next to evaluate the additional parameters, A_K, E_K, and n, needed to define the TTT diagram, the experimental terms in the Kissinger Eq. [15] are fitted by linear regression. A precondition that must be fulfilled, to use this equation, is that the extent of crystallization at the maximum of each peak, x_m, given by Eq. [13] and illustrated in Figure 5(a), should be a constant, independent of $|\phi|$. Table IV lists the average x_m values, over the different $|\phi|$, determined for each of the peaks in the DSC traces of slags A and B. It is observed that the average x_m varied from peak to peak, but for each of them varied little with $|\phi|$, the standard deviations where ~0.06 to 0.10.[75] Hence, it was assumed that the Kissinger method could be applied to the crystalline transformation(s) occurring in each devitrification and crystallization peak.

The Kissinger lines for each of the peaks appearing in the devitrification and crystallization tests are presented, respectively, in Figures 7(a) and (b) for both glasses. From figures, is seen that the experimental $\ln(|\phi|/T_m^2)$ *vs* $1/T_m$ points are fitted very well by straight lines. The kinetic parameters E_K, A_K and n evaluated for each of the peaks are reported in figure legends. These values were used to evaluate the second term on the r.h.s. of Eq. [18] needed to calculate TTT diagrams.

In some works it has been assumed that the activation energy alone can reflect the tendency of a slag to crystallize, a lower energy value would mean a smaller barrier to form ordered structures.[45,47] However, in this work the E_K values found for the most prominent heating, $P_{h,1}$, and cooling, $P_{c,1}$, peaks were larger for slag B than for slag A, despite that the first crystallizes faster, as seen in Section IV–C. This was also the case of the modified activation energies corresponding to the induction periods of peaks $P_{h,1}$ and $P_{c,1}$, as seen in Table IV. From these findings it is conjectured that since the kinetic models depend on many empirical quantities, *i.e.*, on A_1', B_i, A_K, E_K and n, the tendency to crystalize must be evaluated from the time required to achieve a certain degree of crystallization instead from just one kinetic parameter.

Table II. X-Ray Diffraction Results Showing the Crystalline Phases and Their Relative Fractions, Formed in Mold Glass A Under Different Thermal Conditions

Temperature–Time Conditions		*Crystalline Phases Precipitated (pct)		
T [K (°C)]	t (min)	Cus	Com	Amo
Quasi-isothermal devitrification tests with temperature plateau within the range of the DSC devitrification peaks with $\phi_h = 0.33$ K/s (20 °C/min), $\phi_c = -8.33$ K/s (500 °C/min)				
898 (625)	1	✔	—	✔
923 (650)	1	✔	—	✔
948 (675)	1	97.75	2.25	✔
948 (675)	5	87.26	12.74	—
Isothermal treatments				
874 (601)	12	✔	—	—
874 (601)	16	96.51	3.49	—
874 (601)	22	92.66	7.34	—
873 (600)	44	87.25	12.75	—
916 (643)	11	81.13	18.87	—
916 (643)	22	75.79	24.21	—
916 (643)	44	73.66	26.34	—
948 (675)	1	✔	—	✔
973 (700)	1	✔	—	✔
1173 (900)	11	74.48	25.52	—
1173 (900)	88	73.17	26.83	—

Data collected by Cu radiation in the angular range of 7 to 100 deg 2θ with a step size of 0.025 deg 2θ and a counting time of 16.5 s/step, at room temperature.

*Cus—cuspidine, $Ca_4Si_2O7F_{1.5}(OH)_{0.5}$; Com—combeite, $Na_2Ca_2Si_3O_9$; Amo—amorphous.

✔ Present.

Table III. X-Ray Diffraction Results Showing the Crystalline Phases and Their Relative Fractions, Formed in Mold Glass B Under Different Thermal Conditions

Temperature–Time Conditions		*Crystalline Phases Precipitated (pct)				
T [K (°C)]	t (min)	Cus	Qrt	SAS1	Mul	Amo
Quasi-isothermal devitrification tests with temperature plateau within the range of the DSC devitrification peaks with $\phi_h = 0.33$ K/s (20 °C/min), $\phi_c = -8.33$ K/s (500 °C/min)						
883 (610)	1	60.59	21.02	10.41	7.99	✔
893 (620)	1	79.80	4.54	13.21	2.44	✔
903 (630)	1	81.27	2.49	14.81	1.39	✔
903 (630)	5	84.35	0.68	14.97	—	—

Temperature–Time Conditions		*Crystalline Phases Precipitated (pct)					
T [K (°C)]	t (min)	Cus	Nep	SAS1	SAS2	Qrt	Vil
Isothermal treatments							
862 (589)	11	84.4	—	13.5	—	0.7	1.5
862 (589)	22	85.9	—	11.7	—	0.6	1.8
1023 (750)	11	80.4	9.4	6.0	2.0	—	2.2
1173 (900)	11	82.0	5.3	9.3	1.6	—	1.9
1223 (950)	30	79.7	4.0	13.2	1.3	—	1.8

Data collected by Cu radiation in the angular range of 7 to 100 deg 2θ with a step size of 0.025 deg 2θ and a counting time of 16.5 s/step, at room temperature.

*Cus—cuspidine, $Ca_4Si_2O7F_{1.5}(OH)_{0.5}$; Nep—nepheline, $NaAlSiO_4$; SAS1—sodium aluminosilicate, $Na_8Al_4Si_4O_{18}$; SAS2—sodium aluminosilicate, $Na_6(AlSiO_4)_6$; Qua- quartz, SiO_2; Mul—mullite, $Al_{4.52}Si_{1.48}O_{9.74}$; Vil—villiaumite, NaF; Amo: amorphous.

✔ Present.

As Šimon[68] has clearly pointed out E_K, like the other parameters, is just an adjustable parameter that in general does not have a clear physical meaning and one should be very cautious when trying to give mechanistic sense to it, something which is not uncommon in the literature. In another work by Šimon *et al.*[69] the difference in stability of different glasses was attributed to a disparity in A_1' values since the modified activation energy, B, was approximately constant for the samples studied. Branda *et al.*[77] also found that a smaller activation energy does

not necessarily indicate a greater tendency to crystallize. A better form of estimating this trend is by assessing the variation of the degree of crystallization with time at the temperatures of interest, as is done in Section IV–C.

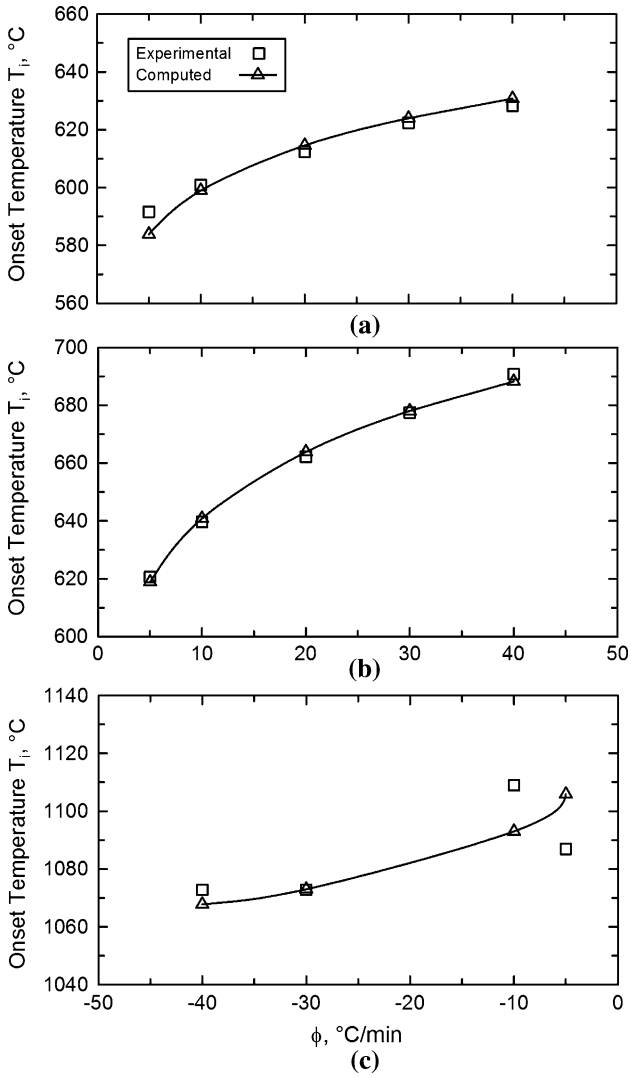

Fig. 6—Comparison between measured and computed onset temperatures for mold slag A as a function of heating rate for (*a*) peak 1 and (*b*) peak 2, of devitrification and (*c*) for the peak appearing on crystallization at different cooling rates.

C. *DSC-Based TTT Diagrams and Their Validation*

Figures 8(a) and (b) present the TTT diagrams calculated from Eq. [18] for slags A and B, respectively. The calculated lines correspond to conversion fractions, x, equal to 0.01 and 0.99 of the crystalline phases associated with each of the peaks appearing on the DSC traces. For both slags, the estimated TTT diagrams predict that over a certain intermediate temperature range, the isothermal transformation starts very quickly. However, the nose tip is considerably larger for slag B than for slag A, indicating its higher tendency to crystallize very rapidly over a wider temperature range. According to its diagram slag B starts crystallization in <0.6 seconds (<0.01 minutes) at temperatures between 983 K and 1338 K (710 °C to 1065 °C); this range is considerably narrower for slag A. The line for $x = 0.01$ corresponding to $P_{h,1}$ (peak 1 of heating devitrification) is slightly displaced farther to the right in the case of slag A than in case of slag B, and this displacement is more noticeable for the curves associated to $P_{c,1}$ (peak 1 of cooling crystallization). In particular, the line marking the end of crystallization (*i.e.*, $x = 0.99$) of the crystalline phase(s) associated with $P_{c,1}$ is reached in a considerably shorter time for slag B than for slag A.

Figures 9 and 10 show the microstructures found in the region close to the hot surface (≤50 μm from it) of disks treated on the Inconel plate illustrated in Figure 2, the photomicrographs indicate the temperatures prevailing in that region for the time indicated. These conditions are denoted by the x symbols plotted in Figures 8(a) and (b) to compare qualitatively microstructures against expected transformations. At 773 K (500 °C) the photomicrographs shows that glass samples of both slags stayed glassy after 7200 seconds (120 minutes) of treatment, which agrees with their respective TTT diagram. At 873 K (600 °C) the same happened for $t = 20$ seconds (0.33 minutes); while for 80 seconds (1.33 minutes) small crystal grains are observed in the photomicrograph of slag B but not in that for slag A, in accordance with the corresponding diagram; at 1320 seconds (22 minutes) of treatment the photomicrographs of both samples show similarity, as expected from the diagrams. For $T = 973$ K (700 °C) and treatment times of 20 seconds (0.33 minutes) and 80 seconds (1.33 minutes) the photomicrographs of the samples of slag A indicate less transformation than the

Table IV. Kinetic Parameters for the Induction Periods of the Peaks Appearing During Heating and Cooling of Mold Slags A and B and Conversions at DSC Peak Maximum

	Devitrification Peaks		Crystallization Peaks			
Powder and Parameters	$P_{h,1}$	$P_{h,2}$	$P_{c,1}$	$P_{c,2}$	$P_{c,3}$	$P_{c,4}$
A						
A_i' (min)	1.3×10^{-16}	1.4×10^{-11}	1.5×10^{-33}	—	—	—
B_i (K)	32,618	23,919	−103,520	—	—	—
x_m	0.93	0.31	0.62	—	—	—
B						
A_i' (min)	3.8×10^{-19}	—	6.8×10^{49}	3.4×10^{32}	5.6×10^{16}	8.62×10^{15}
B_i (K)	37,210	—	−159,851	−88,890	−42,720	−31,731
x_m	0.55	—	0.41	0.38	0.43	0.50

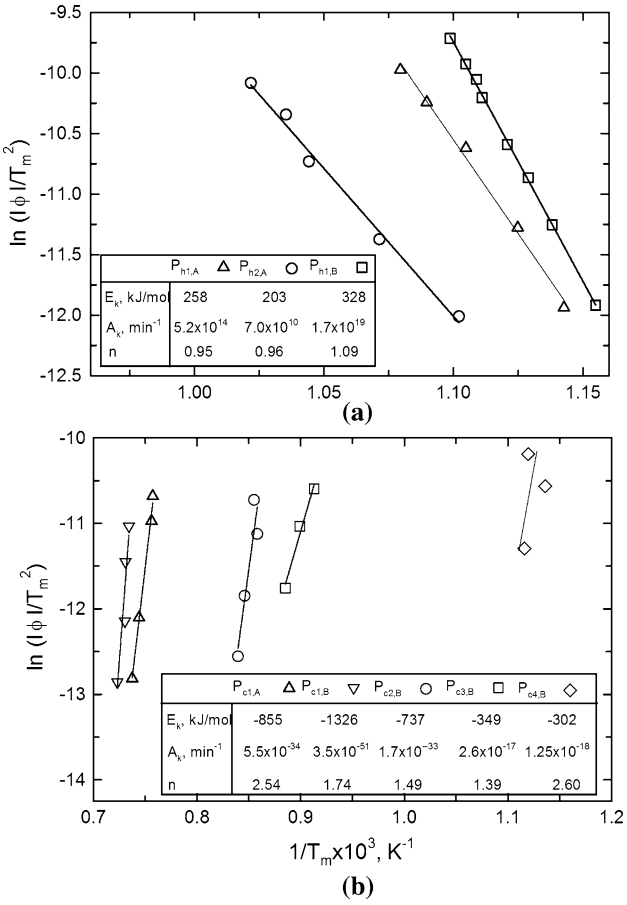

Fig. 7—Kissinger lines for slags A and B corresponding to: (*a*) devitrification and (*b*) crystallization. The estimated kinetic parameters are given in the legends.

samples of slag B which again agrees with the respective TTT diagrams; at 1320 seconds (22 minutes) the photomicrographs of both slags look alike.

At 1073 K (800 °C) with a treatment (holding) time of 20 seconds (0.33 minutes), the devitrification lines that comprise the bottom half of the TTT diagrams indicate almost complete transformation for slag A and complete transformation for slag B; while for the treatments lasting 300 seconds (5 minutes) both slags devitrified completely. Full devitrification of both glasses is predicted at 1173 K (900 °C) for the two holding times used, 20 and 300 seconds (0.33 and 5 minutes). The predictions from the diagrams in Figure 8 agree with the respective microstructures observed in Figures 9 and 10. Also from Figures 8(a) and (b) is seen that the TTT lines of slag B suggest that crystallization continues for much longer times than the crystallization processes in slag A.

To evaluate how effective is the analysis proposed in this work to determine the evolution of different crystalline phases, the slag powdered samples treated isothermally in a muffle furnace, as indicated in Section III–C, were analyzed by X-ray diffraction and the relative proportion of the crystalline phases was determined by the Rietveld method. The temperatures and times of the treatments carried out on samples of slag A are reported in Table II together with the X-ray diffraction results and the set of conditions are represented by the triangles plotted in Figure 8(a). According to table for a temperature of 874 K (660 °C) and $t = 720$ seconds (12 minutes) only cuspidine was found as expected from the diagram in Figure 8(a). For the same temperature but for holding times of 960, 1320, and 2640 seconds (16, 22, and 44 minutes), the percentage of combeite in the samples increased with time in agreement with the diagram; the cuspidine does not decompose, its relative percentage decreases as a result of the increase in combeite with time. In the case of the treatments at 916 K (643 °C), the table indicates an increase in combeite as the diagram also indicates. It should be noticed that for the treatments at 916 K (643 °C) with times of 1320 and 2640 seconds (22 and 44 minutes) and at 1173 K (900 °C) with times of 660 and 5280 seconds (11 and 88 minutes), the percentages of cuspidine and combeite are very close, indicating, in agreement with the TTT diagram, that in all the cases the crystalline transformations had been completed. In the samples treated isothermally at 948 K and 973 K (675 °C and 700 °C) for 60 seconds (1 minute), the table indicates that the phases found were cuspidine and glass, which agrees with the predictions of the TTT diagram.

In the case of slag B, many different crystalline phases precipitated and the devitrification/crystallization processes were much more complex, as seen in Table III and Figure 8(b). Therefore, it is complicated to carry out a description such as that given in the previous paragraph for slag A. Table III indicates that at the lower temperature, 862 K (589 °C), and for times between the TTT lines, calculated from the only DSC peak appearing during devitrification, four crystalline phases develop, but these were not exactly the same as those obtained in the quasi-isothermal tests which are reported in the upper part of table. Also, from table is seen that at the higher temperatures [1023 K, 1173 K, 1223 K (750 °C, 900 °C, 950 °C)], more crystalline phases were found and their percentages at each condition were different. The fact that the percentages were different suggest that crystallization kept evolving, as would seemingly indicate the spread out of the transformation lines over the diagram displayed in Figure 8(b).

In agreement with the literature, the DSC-based technique developed in this work to calculate TTT diagrams shows that glass B, with higher basicity, exhibited a higher tendency to crystallize. As seen in Table I, this higher basicity is due to glass B containing less SiO_2 than glass A, as both had similar CaO concentration. The higher basicity would lead to shorter silicate networks, causing a lower viscosity, which favors the diffusion processes required to form crystalline phases. An additional effect could be expected from the higher concentration of F and MnO in glass B compared to glass A, since these species also cause slag viscosity to decrease.[42,44,45,78] Furthermore, the higher concentration of F in glass B might enhance the formation of cuspidine, $Ca_4Si_2O7F_{1.5}(OH)_{0.5}$, and then villiaumite, NaF; which did not appear in the devitrification of glass A. Finally, the much-higher concentration of Al_2O_3 in glass B might have been responsible for

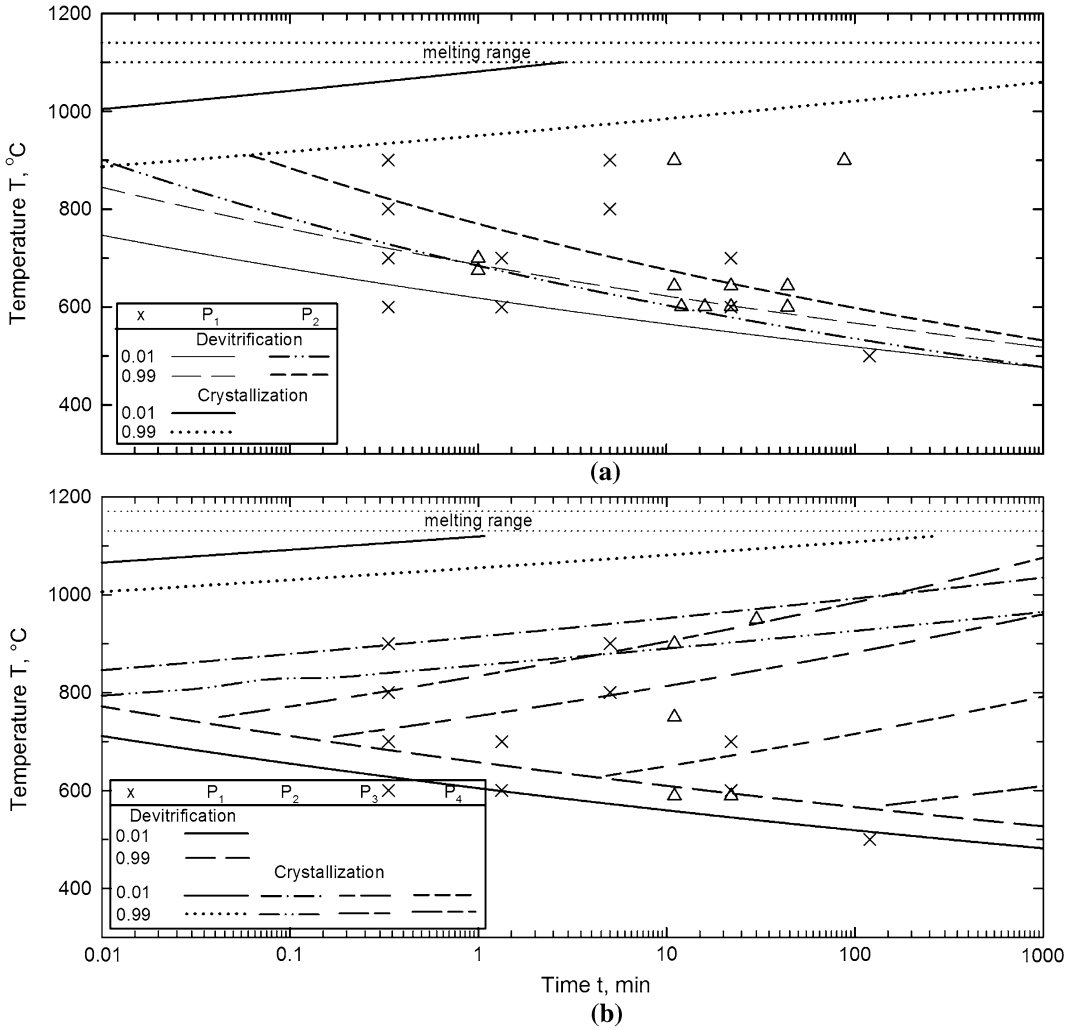

Fig. 8—TTT diagrams calculated for: (*a*) slag A and (*b*) slag B.

the large number of aluminosilicate phases that formed during the isothermal treatment of this glass, as reported in Table III. The formation of so many different crystalline phases made the TTT diagram of slag B much more complex than that of slag A.

V. SUMMARY AND CONCLUSIONS

Differential thermal calorimetry allows quick determination of important properties over a wide range of temperatures, using only a small amount of sample and an instrument that is easily available in most laboratories. To better quantify the crystallization of mold slags during continuous casting of steel, this work extends the non-isothermal DSC test using the Induction Period (of Šimon and Kolman) and Kissinger methods to evaluate the following expression,

$$t = t_i + \left(\frac{1-(1-x)^{1-n}}{[A_K e^{-B_K/T}]}\right)\left(\frac{1}{1-n}\right) \qquad [18]$$

proposed to estimate TTT diagrams. The standard kinetic methods were expanded to estimate: t_i, A_K, B_K, and n, from crystallization peaks appearing on thermograms obtained during cooling of liquid slags at various constant rates, and not only from thermograms obtained during heating of a glassy material at various linear rates, as has been done previously for devitrification. The experimental data needed for this purpose are onset temperature, T_i, peak maximum temperature, T_m, shape index, S, and conversion at peak maximum, x_m, collected at various constant heating and cooling rates.

These data were gathered to investigate the crystallization kinetics of two mold slags, one for casting low-carbon steels and the other for casting medium-carbon steels. The results obtained correctly portray their different crystallization behavior, *i.e.*, delayed crystallization of the slag for low-carbon steels relative to the slag for medium-carbon steels. The TTT diagrams include the curves for the start and end of transformation of the crystalline phase(s) forming at each DSC crystallization peak, thus they describe in detail the transformations taking place. The TTT diagrams esti-

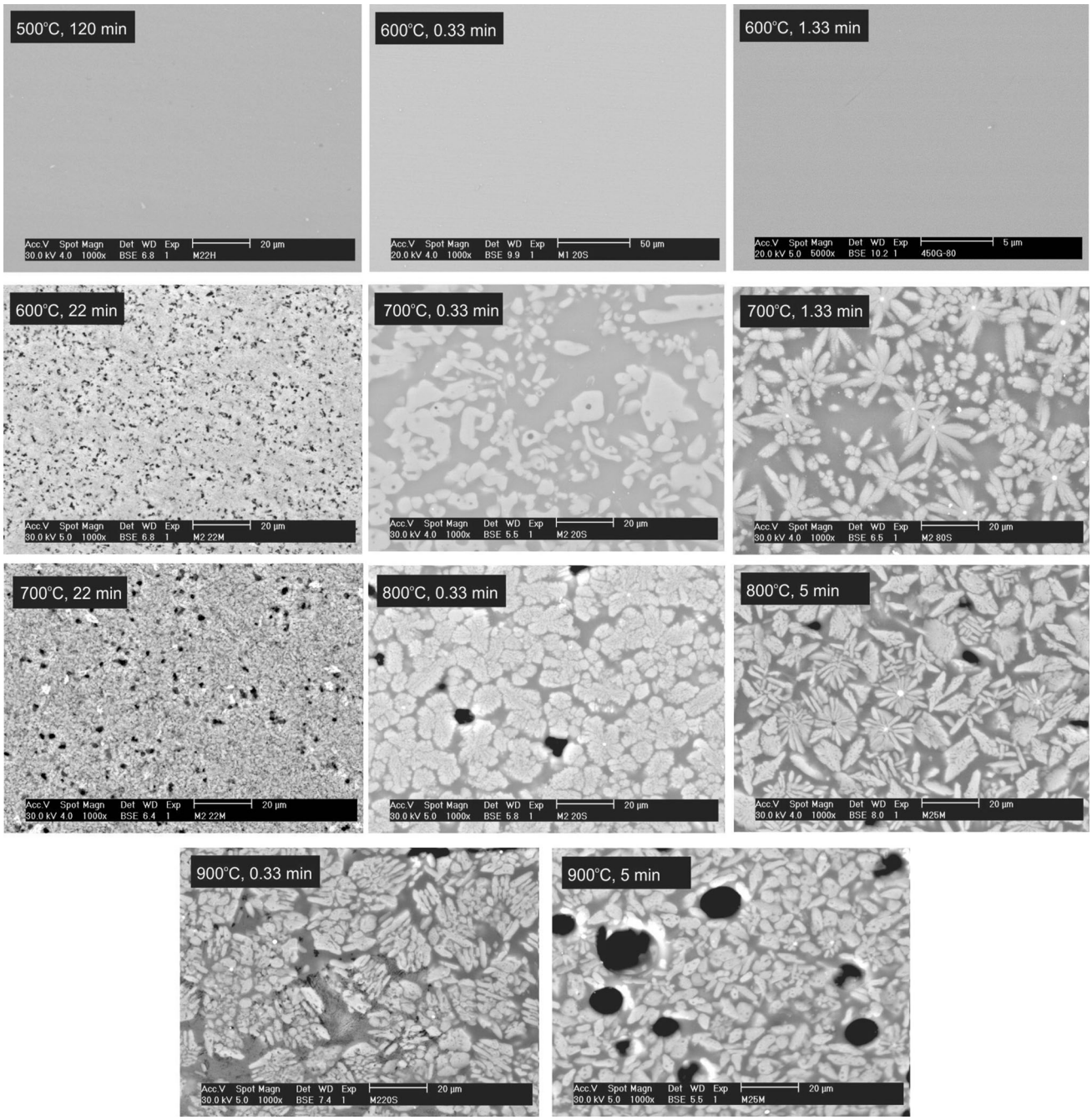

Fig. 9—Backscattered electron photomicrographs of regions close to the hot surface of disks of slag A devitrified isothermally at the conditions indicated.

mated with the new DSC-based procedure developed in this work agree well with independent isothermal transformations results approximated by heating glass disks (~3 mm thick) on a hot pan, holding isothermally for specified time intervals, quenching and examining with a SEM. Significantly, the expected transformations also match with quantitative X-ray diffraction measurements carried out on powder samples of mold glass treated isothermally in a muffle furnace.

New results obtained using our new CLSM facility, in combination with SEM–EDS and XRD techniques for the identification of the crystalline phases, agree with the results obtained from the DSC-based TTT diagrams. The outcome of this investigation will be reported elsewhere.

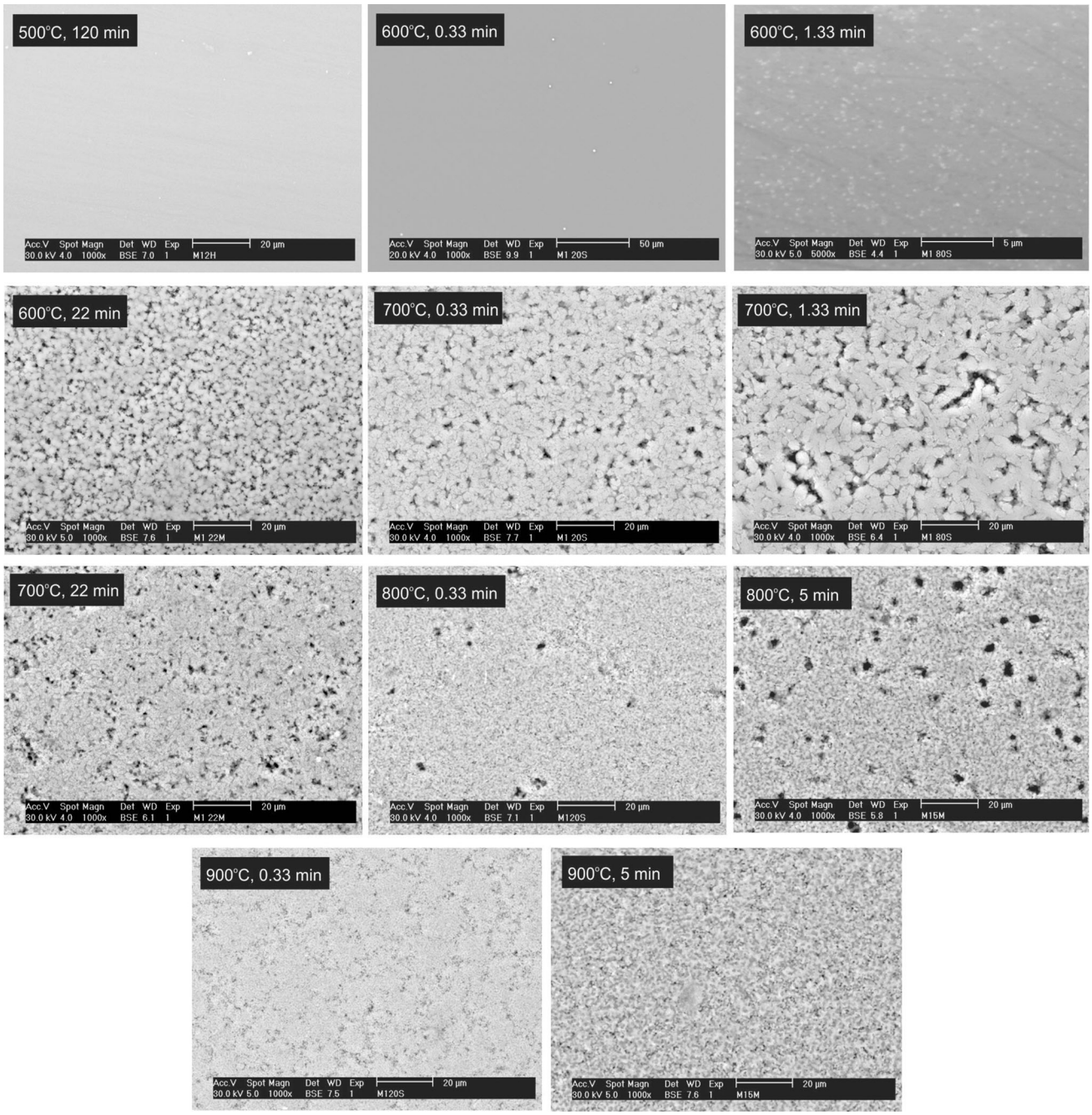

Fig. 10—Backscattered electron photomicrographs of regions close to the hot surface of disks of slag B devitrified isothermally at the conditions indicated.

ACKNOWLEDGMENTS

We are grateful to the Centro de Investigación y de Estudios Avanzados (CINVESTAV – Unidad Saltillo) and the Continuous Casting Consortium at the University of Illinois for financial support. YGM and CBP are grateful to the National Council of Science and Technology of México (CONACYT) for the Ph.D. and M.Sc. scholarship grants received.

NOMENCLATURE

A	Frequency factor, min^{-1}
A_i'	Modified frequency factor, min
B	Modified activation energy, K
E	Activation energy, J mol^{-1}
f	Kinetic function depending only on degree of conversion
k	Function depending on temperature with the form of Arrhenius expression, min^{-1}

n	Order of reaction
P	Peak
R	Gas constant, 8.31 J mol^{-1} K^{-1}
S	Peak shape index; area between DSC peak and baseline
t	Time, s or min
T	Temperature, K (°C)
x	Degree of conversion
ϕ	Heating or cooling (−) rate, K/s or °C/min

SUBSCRIPT

c	Cooling
h	Heating
i	End of induction period or onset of crystallization; denote a quantity appearing in IP method
K	Denote a quantity appearing in Kissinger method
L	Liquidus
m	Denote quantity at DSC peak maximum
T	Total
1,2,3,4	Peak number from start of heating or from start of cooling

REFERENCES

1. J.K. Brimacombe and K. Sorimachi: *Metall. Trans B.*, 1977, vol. 8B, pp. 489–505.
2. A. Grill, K. Sorimachi, and J.K. Brimacombe: *Metall. Trans. B*, 1976, vol. 7B, pp. 177–89.
3. B.G. Thomas, J. Bentsman, B. Petrus, X. Zhou, K. Zheng, S. Vapalahti, H. Li, and A.H. Castillejos: *Proc. 2009 NSF Eng. Res. Innov. Conf.*, Honolulu, Hawaii, grant #DMI-0500453.
4. W.H. Emling: *The Making, Shaping and Treating of Steel*, A.W. Cramb, ed., The AISE Steel Foundation, Pittsburgh, PA., 2003, pp. 1–34.
5. K.C. Mills, A.B. Fox, Z. Li, and R.P. Thackray: *Ironmak. Steelmak.*, 2005, vol. 32, pp. 26–34.
6. R.J.O'Malley and J. Neal: *Proc. METEC Congress 99*, Dusseldorf, 1999, vol. 1, pp. 188–95.
7. B. Stewart, M. McDonald, M. Hopkins, and R. Burniston: *Proc. Conf. Eur. Contin. Cast. Steel*, Riccione, Italy, 3–6 June, 2008, pp. 55–62.
8. W. Yan, W.Q. Chen, C. Lippold, and H.G. Zheng: *La Metallurgia Italiana*, 2013, pp. 35–42.
9. Y. Meng and B.G. Thomas: *ISIJ Int.*, 2006, vol. 46, pp. 660–69.
10. P.O. Hooli: *Ironmak. Steelmak.*, 2002, vol. 29, pp. 293–96.
11. V. Ludlow, B. Harris, S. Riaz, and A. Normanton: *Proc. VII Int. Conf. Molten Slags Fluxes Salts*, Johannesburg, South Africa, 2004, pp. 723–30.
12. J.A. Kromhout, S. Melzer, E.W. Zinngrebe, A.A. Kamperman, and R. Boom: *Steel Res.*, 2008, vol. 79, pp. 143–48.
13. L. Zhou, W. Wang, D. Huang, J. Wei, and J. Li: *Metall. Mater. Trans. B*, 2012, vol. 43B, pp. 925–36.
14. J.W. Cho and H. Shibata: *J. Non-Cryst. Solids*, 2011, vol. 282, pp. 110–17.
15. J.W. Cho, T. Emi, H. Shibata, and M. Suzuki: *ISIJ Int.*, 1998, vol. 38, pp. 834–42.
16. J. Cho, H. Shibata, T. Emi, and M. Suzuki: *ISIJ Int.*, 1998, vol. 38, pp. 440–46.
17. J. Cho, H. Shibata, T. Emi, and M. Suzuki: *ISIJ Int.*, 1998, vol. 38, pp. 268–75.
18. K. Gu, W. Wang, L. Zhou, F. Ma, and D. Huang: *Metall. Mater. Trans. B*, 2012, vol. 43B, pp. 937–45.
19. J. Diao, B. Xie, and J.P. Xiao: *Ironmak. Steelmak.*, 2009, vol. 36, pp. 610–14.
20. H. Kyoden, T. Doihara, and O. Nomura: *69th Steelmak. Conf. Proc.*, Washington, DC, vol. 69, 1986, pp. 153–59.
21. Y. Meng, B.G. Thomas, A.A. Polycarpou, A. Prasad, and H. Henein: *Can. Metall. Q.*, 2006, vol. 45, pp. 79–94.
22. J.E. Camporredondo S., A.H. Castillejos E., F.A. Acosta G., E.P. Gutierrez M., and M.A. Herrera G., *Metall. Mater. Trans. B*, 2004, vol. 35B, pp. 541–60.
23. K.C. Mills, L. Courtney, A.B. Fox, B. Harris, Z. Idoyaga, and M.J. Richardson: *Thermochim. Acta*, 2002, vol. 391, pp. 175–84.
24. R.W. Soares, M.V.A. Fonseca, R. Neuman, V.J. Menezes, A.O. Lavinas, and J. Dweck: *Thermochim. Acta*, 1998, vol. 318, pp. 131–36.
25. R.V. Branion, D.A. Dukelow, G.D. Lawson, J. Schade, M. Schmidt, and H.T. Tsai: *78th Steelmak. Conf. Proc.*, Nashville, vol. 78, 1995, pp. 647–53.
26. M.J. Frazee: *78th Steelmak. Conf. Proc.*, Nashville, vol. 78, 1995, pp. 639–45.
27. Z. Li, R. Thackray, and K.C. Mills: *Proc. VII Int. Conf. Molten Slags Fluxes Salts*, Johannesburg, South Africa, 2004, pp. 813–19.
28. K. Watanabe, M. Suzuki, K. Murakami, H. Kondo, and T. Shiomi: *79th Steelmak. Conf. Proc.*, Pittsburgh, vol. 79, 1996, pp. 265–68.
29. P. Rocabois, J.N. Pontoire, J. Lehmann, and H. Gaye: *J. Non-Cryst. Solids*, 2001, vol. 282, pp. 98–109.
30. Y. Kashiwaya, C.E. Cicutti, and A.W. Cramb: *ISIJ Int.*, 1998, vol. 38, pp. 357–65.
31. L. Zhou, W. Wang, F. Ma, J. Li, J. Wei, H. Matsuura, and F. Tsukihashi: *Metall. Mater. Trans. B*, 2012, vol. 43B, pp. 354–62.
32. W. Guang-hau, L. Hui, and T. Ping: *J. Iron Steel Res. Int.*, 2008, vol. 15, pp. 32–37.
33. Y. Kashiwaya, T. Nakauchi, K.S. Pham, S. Akiyama, and K. Ishii: *ISIJ Int.*, 2007, vol. 47, pp. 44–52.
34. Y. Kashiwaya, C.E. Cicutti, A.W. Cramb, and K. Ishii: *ISIJ Int.*, 1998, vol. 38, pp. 348–56.
35. C. Orrling and A.W. Cramb: *I&SM*, 2000, vol. 27, pp. 53–63.
36. C. Orrling and A.W. Cramb: *Metall. Mater. Trans. B*, 2000, vol. 31B, pp. 403–06.
37. C.T. Mutale, T. Claudon, and A.W. Cramb: *Metall. Mater. Trans. B*, 2005, vol. 36B, pp. 417–18.
38. L. Zhou, W. Wang, R. Liu, and B.G. Thomas: *Metall. Mater. Trans. B*, 2013, vol. 44B, pp. 1264–79.
39. H. Mizuno, H. Esaka, K. Shinozuka, and M. Tamura: *ISIJ Int.*, 2008, vol. 48, pp. 277–85.
40. S.S. Jung and I. Sohn: *Metall. Mater. Trans. B*, 2012, vol. 43B, pp. 1530–39.
41. Z. Zou-tai, L. Jing, and L. Peng: *J. Iron Steel Res. Int.*, 2011, vol. 18, pp. 31–37.
42. J-Y. Park, J.W. Ryu, and I. Sohn: *Metall. Mater. Trans. B*, 2014, vol. 45B, pp. 1186–91.
43. J.V. Dubrawski and J.M. Camplin: *J. Therm. Anal.*, 1993, vol. 40, pp. 329–34.
44. R. Carli and V. Ghilardi: *I&SM*, 1998, vol. 25, pp. 43–46.
45. R. Carli and C. Righi: *Proc. VII Int. Conf. Molten Slags Fluxes Salts*, Johannesburg, South Africa, 2004, pp. 821–26.
46. R.G. Hill, N.D. Costa, and R.V. Law: *J. Non-Cryst. Solids*, 2005, vol. 351, pp. 69–74.
47. M. Dapiaggi, G. Artioli, C. Righi, and R. Carli: *J. Non-Cryst. Solids*, 2007, vol. 353, pp. 2852–60.
48. R. Bommaraju: *74th Steelmak. Conf. Proc.*, Washington, DC, 1991, pp. 131–46.
49. S. Mackay, N.S. Hunter, A.S. Normanton, V. Ludlow, P.N. Hewitt, and B. Harris: *Ironmak. Steelmak.*, 2002, vol. 29, pp. 185–90.
50. S.P. He, Q. Wang, D. Xie, C.S. Xu, Z.S. Li, and K.C. Mills: *Int. J. Miner. Metall. Mater.*, 2009, vol. 16, pp. 261–64.
51. C.S. Ray, S.T. Reis, R.K. Brow, W. Höland, and V. Rheinberger: *J. Non-Cryst. Solids*, 2005, vol. 351, pp. 1350–58.
52. P. Gabbot: *A Practical Introduction to Differential Scanning Calorimetry, Chap. 1*, http://media.johnwiley.com.au/product_data/excerpt/13/14051317/1405131713.pdf.
53. H.E. Kissinger: *J. Res. Natl. Bur. Stand.*, 1956, vol. 57, pp. 217–21.
54. H.E. Kissinger: *Anal. Chem.*, 1957, vol. 29, pp. 1702–06.
55. K Matusita and S Sakka: *J. Non-Cryst. Solids*, 1980, vols. 38–39, pp. 741–46.

56. K. Matusita and S. Sakka: *Bull. Inst. Chem. Res*, 1981, vol. 59, pp. 159–70.
57. J.H. Flynn: *J. Therm. Anal.*, 1983, vol. 27, pp. 95–102.
58. L.V. Meisel and P.J. Cote: *Acta Metall.*, 1983, vol. 31, pp. 1053–59.
59. J.P. Elder: *J. Therm. Anal.*, 1985, vol. 30, pp. 657–69.
60. J.M. Criado and A. Ortega: *J. Non-Cryst. Solids*, 1986, vol. 87, pp. 302–11.
61. N. Sbirrazzuoli, Y. Girault, and L. Elégant: *Thermochim. Acta*, 1997, vol. 293, pp. 25–37.
62. S. Vyazovkin and C.A. Wight: *Int. Rev. Phys. Chem.*, 1998, vol. 17, pp. 407–33.
63. P. Budrugeac and E. Segal: *J. Therm. Anal. Calorim.*, 2007, vol. 88, pp. 703–07.
64. P.E. Sánchez-Jiménez, J.M. Criado, and L.A. Pérez-Maqueda: *J. Therm. Anal. Calorim.*, 2008, vol. 94, pp. 427–32.
65. R.L. Blaine and H.E. Kissinger: *Thermochim. Acta*, 2012, vol. 540, pp. 1–6.
66. T. Ozawa: *Bull. Chem. Soc. Jpn.*, 1984, vol. 57, pp. 639–43.
67. P. Šimon and L'. Kolman: *J. Therm. Anal. Calorim.*, 2001, vol. 64, pp. 813–20.
68. P. Šimon: *J. Therm. Anal. Calorim.*, 2005, vol. 82, pp. 651–57.
69. P. Šimon, K. Nemčeková, E. Jóna, A. Plško, and D. Ondrušová: *Thermochim. Acta*, 2005, vol. 428, pp. 11–14.
70. P. Šimon: *J. Therm. Anal. Calorim.*, 2006, vol. 84, pp. 263–70.
71. P. Šimon, E. Illeková, and S.C. Mojumdar: *J. Therm. Anal. Calorim.*, 2006, vol. 83, pp. 67–69.
72. J.A. Nelder and R. Mead, http://comjnl.oxfordjournals.org/, Accessed 22 April 2014.
73. A program for function minimization using the SIMPLEX method, programed by D.E. Shaw, amended by A. Miller, http://www.nist.gov/pml/div684/grp03/upload/NelderMeadMinimizer.f90, Accessed 22 April 2014.
74. Y.G. Maldonado, A. Humberto Castillejos, and B.G. Thomas: *Iron Steel Technol.*, 2013, vol. 10, pp. 65–75.
75. Y.G. Maldonado, Ph.D. Thesis to be presented, CINVESTAV–Unidad, Saltillo. Coahuila, Mexico, 2014.
76. F. Branda, A. Buri, A. Marotta, and S. Saillo: *J. Mater. Sci. Lett.*, 1984, vol. 3, pp. 654–58.
77. F. Branda, A. Marotta, and A. Buri: *J. Non-Cryst. Solids*, 1991, vol. 134, pp. 123–28.
78. G.-H. Zhang, K-Ch. Chou, Q.-G. Xue, and K.C. Mills: *Metall. Mater. Trans. B*, 2012, vol. 43B, p. 64.